HIFAN 1711

Designing Neutralized Drift Compression for Focusing of Intense Ion Beam Pulses in a Background Plasma

by
I.D. Kaganovich, R.C. Davidson, M. Dorf, E.A. Sefkow, PPPL
J.J. Barnard, A. Friedman, LLNL
E.P. Lee, S.M. Lidia, B.G. Logan, P.K. Roy, P.A. Seidl, LBNL
D.R. Welch Voss Scientific

Accelerator Fusion Research Division
Ernest Orlando Lawrence Berkeley National Laboratory
University of California
Berkeley, California 94720

Date
May 2009

This work was supported by the Director, Office of Science, Office of Fusion Energy Sciences, of the U.S. Department of Energy under Contract No. DE-AC02-05CH11231.

DESIGNING NEUTRALIZED DRIFT COMPRESSION FOR FOCUSING OF INTENSE ION BEAM PULSES IN BACKGROUND PLASMA*

I. D. Kaganovich, R.C. Davidson, M. Dorf, E. A. Startsev, A. B. Sefkow, Plasma Physics Laboratory, Princeton University, Princeton, New Jersey 08543, U.S.A
J. J. Barnard, A. Friedman, E.P. Lee, S.M. Lidia, B.G. Logan, P.K. Roy, P. A. Seidel, Lawrence Berkeley National Laboratory, Berkeley, California, 94720, USA
D. R. Welch, Voss Scientific Inc., Albuquerque, NM 87108, USA

Abstract

Neutralized drift compression offers an effective method for particle beam focusing and current amplification. In neutralized drift compression, a linear radial and longitudinal velocity drift is applied to a beam pulse, so that the beam pulse compresses as it drifts in the drift-compression section. The beam intensity can increase more than a factor of 100 in both the radial and longitudinal directions, resulting in more than 10,000 times increase in the beam number density during this process. The self-electric and self-magnetic fields can prevent tight ballistic focusing and have to be neutralized by supplying neutralizing electrons. This paper presents a survey of the present theoretical understanding of the drift compression process and plasma neutralization of intense particle beams. The optimal configuration of focusing and neutralizing elements is discussed in this paper.

INTRODUCTION

An effective way to achieve high current density of an ion beam pulse on a target is to simultaneously compress the beam in both the radial and longitudinal direction. This is accomplished by applying a velocity tilt to a beam pulse, so that the beam tail is accelerated relative to the beam head. As a result, the beam number density increases during the drift compression, when the beam tail approaches the beam head. Similarly, the beam pulse can be compressed radially by passing the beam pulse through a focusing element. Because the self-electric field of the beam increases rapidly during compression, the beam space charge may prevent the beam from compression, and thus has to be effectively neutralized. A schematic of the beam compression is shown in Fig.1. In this paper we review the conceptual design of the neutralized drift compression system and analyze the factors that may prevent achieving high compression. This paper is organized as follows. The discussion is split according to components of the neutralized drift compression: the longitudinal compression, the radial and simultaneous compression; and the physics of the neutralization process.

LONGITUDINAL COMPRESSION

Longitudinal compression is accomplished by accelerating the tail of the beam relative to the head of the beam. This is accomplished experimentally by passing the beam through a time-dependent acceleration module. For the Neutralized Drift Compression eXperiment (NDCX) [1,2,3], the accelerating module is the induction bunching module. The module consists of many independently-driven magnetic cores that generate an inductive electric field, which is applied to two electrodes, as shown in Fig.2.

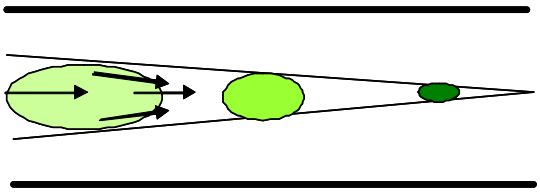

Figure 1: Schematic of beam compression. Arrows indicate the direction of the local beam velocity.

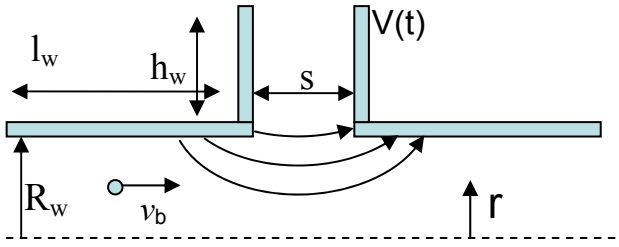

Figure 2: Schematic of the acceleration gap of the inductive bunching module . Arrows indicate the direction of the electric field; the dotted line shows the axis of symmetry.

The resulting change in the beam velocity $\Delta v_b(\tau)$ should be chosen so that all beam ions during the pulse in the interval $0 \le \tau \le t_p$ arrive at the same focal plane at a distance L_f from the induction bunching module. The beam trajectory is given by

$$z(t,\tau) = v_b(\tau)(t-\tau)\,, \qquad (1)$$

where $v_b(\tau) = v_{b0} + \Delta v_b(\tau)$ is the beam velocity after the bunching module, and v_{b0} is the initial beam velocity before the bunching module. The condition for longitudinal compression is that all parts of the

*Research supported by the U.S. Department of Energy
#ikaganov@pppl.gov

compressed beam pulse arrive simultaneously at the same location, i.e., $z(t_f,\tau)=L_f$, for all τ. Here, $t_f = L_f / v_{b0}$ is time of flight of the beam from the bunching module to the final focus plane. From Equation (1) and $z(t_f,\tau)=L_f$, it follows that the velocity tilt should satisfy [4]

$$\Delta v_b(\tau) = v_{b0}\tau / \left(t_f - \tau\right). \quad (2)$$

Typically, the pulse duration is much shorter than the focusing time, $t_p \ll t_f$, and the velocity modulation is small compared with the initial beam velocity, $|\Delta v_b| < v_{b0}$, with the fractional velocity tilt, $Max(\Delta v_b)/v_{b0}$, of order 1/6-1/3. The ion density can be found from the compression of the beam pulse, dz/dz_0 where dz_0 is initial distances between two slices, and dz is current one. The initial position of a beam ion interacting with the inductive bunching module at time τ is $z_0(\tau) = -v_{b0}\tau$ and the current is given by Eq.(1). Therefore, the ion beam density is

$$n_b(z,t) = n_{b0}\frac{dz_0}{dz} = -\frac{n_{b0}v_{b0}}{\partial z/\partial\tau}.$$

Substituting $z(t,\tau)$ from Eq.(1) gives

$$n_b(z,t) = \frac{n_{b0}v_{b0}}{v_b(\tau) - (t-\tau)d\Delta v_b(\tau)/d\tau}, \quad (3)$$

where τ is determined from Eq.(1) for a given z. Equation (3) can be written in the equivalent form

$$n_b(z,t) = \frac{n_{b0}v_{b0}}{v_b(\tau)\left[1 + \frac{d\ln\left[v_b(\tau)\right]}{d\ln(t-\tau)}\right]}, \quad (4)$$

For the velocity profile given by Eq.(2), the beam density tends to infinity at $t = t_f$, corresponding to perfect compression. If there is an error $\delta v(\tau)$ in the applied velocity then the compression is limited. For a small velocity tilt and error, $|\delta v_b| \ll |\Delta v_b| \ll v_{b0}$, Eq.(3) readily gives the following estimate for maximum compression

$$n_b(z,t_f) = \frac{n_{b0}v_b t_f}{v_b(\tau)\left[\delta v_b(t_f-\tau) + \left(d\delta v_b/d\tau\right)(t_f-\tau)^2\right]}. \quad (5)$$

The first term in the denominator describes the change in the position of a beam slice due to the error in the beam velocity, $\delta z = \delta v_b(\tau)(t_f - \tau)$, whereas the second term describes the relative change between two neighbouring slices. Note that because the velocity error changes with time on a time scale short compared to the focusing time, $t_p << t_f$, the second term typically dominates the first term. Equation (5) was generalized in Refs.[5, 6, 7] taking into account thermal effects and space-charge effects. From Eq.(5) it is evident that the maximum compression is limited by errors in the applied velocity tilt in the induction bunching module compared with the ideal velocity tilt, and is of order

$$C \equiv \max\left(\frac{n_b}{n_{b0}}\right) \sim \frac{1}{\max\left(\frac{\delta v}{v_b}, \frac{t_f}{v_b}\frac{d\delta v_b}{d\tau}\right)} \sim \frac{\Delta v_b}{\delta v_b}. \quad (6)$$

Here, we have used the relationships that $d\delta v/d\tau \sim \delta v/t_p$ and $t_f/t_p \sim v_b/\Delta v_b$. Typical values of the relative error in the induction bunching module, $\delta v_b/\Delta v_b$ are about 1-2%. Equation (6) then gives compression C in the range C~50-100. This estimate agrees well with the reported value of longitudinal compression obtained in experiments [1,2,3]. If there were no error in the velocity tilt, then the effects associated with a small thermal velocity ($T_{bz} \simeq 0.2eV$, say) will limit the compression to a scale of order v_b/v_{bT}~1000, for the 300keV beams characteristic of NDCX-I [3]. However, this would require a very precise designing of the inductive bunching module with an error of order 0.1%; and similarly the control of the beam velocity should be performed with a precision within 0.1%.

RADIAL AND SIMULTANEOUS COMRESSION

Focusing without a final focusing element

If the beam passes through focusing element with a focal plane located at a distance L_f, the typical spot size is determined by the thermal speed, $r_{spot} \sim v_{bT}(L_f/v_b)$, where the term in parenthesis represents the time required for focusing. For NDCX-I parameters, $T_{br} \simeq T_{bz}$, and as discussed above, v_b/v_T~1000, yielding $r_{spot} \sim L_f/1000$. For a meter-scale focusing system, this estimate yields a beam spot radius at the target of about 1mm. Radial compression from an initial beam radius of about 1 cm to a final beam radius on target of about 1mm has been routinely observed in experiments [1], in very good agreement with this estimate. However, some discrepancy occurs when the beam is simultaneously compressed in both the radial and longitudinal directions. The velocity tilt causes the radial focal plane to shift due to the dependence of the focal plane location on the beam velocity. Another difficulty is the focusing effect (aberration) of the induction bunching module.

Aberrations in the induction bunching module

The beam velocity tilt is produced by applying inductively generated voltage to two electrodes, which

are schematically shown in Fig. 2. The electrodes have a hole for beam passage. The hole radius is equal to the accelerator pipe radius, R_w. The hole presence results in producing an electric field profile in the gap that is intrinsically two-dimensional, spreading along the z-direction over distances of order R_w, and producing both radial electric field and longitudinal electric field components. Therefore, together with the velocity change in z-direction, a beam ion acquires a velocity change in the r-direction. In order to calculate the radial velocity change, the radial electric field in the gap must be determined. The electric field in the gap is electrostatic, because the magnetic field is zero inside the gap, and the electric field can be obtained from Poisson's equation, with boundary condition $\phi = 0$ at the left conducting boundary, and $\phi = V(t)$ at the right boundary (see Fig.2). There are analytical solutions for the case of a cylindrical pipe with a gap width s, corresponding to $s<<R_w$, $l_w>>R_w$, and $h_w=0$. Here, l_w is the length of the washer, and h_w is the height of the washer (see Fig.2). The solution of Poisson's equation for the on-axis potential to within 1% accuracy is given by [8]

$$\phi(0,z,t) = \frac{1}{2}V(t)\left[1+\tanh\left(1.32\frac{z}{R_w}\right)\right]. \qquad (7)$$

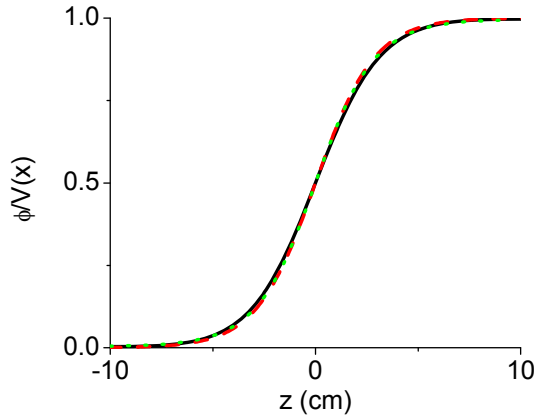

Figure 3: Normalized electrostatic potential profile, ϕ / V, along the gap in NDCX-I device with *s=2.9cm, R_W=3.8cm, l_W=5.08cm*, and *h_W=5.08cm.* The black, solid curve corresponds to the numerical solution; the red, dashed curve corresponds to Eq.(7); and the green, dotted curve corresponds to Eq.(8).

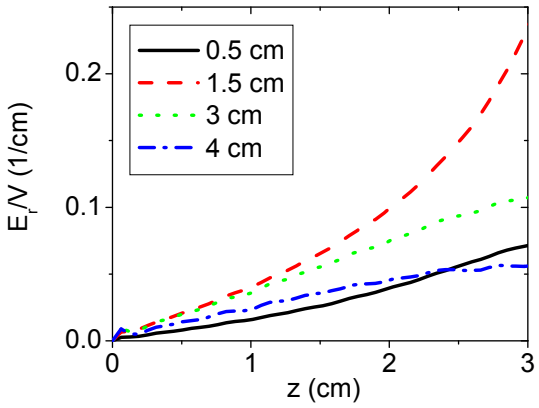

Figure 4: The profile of the normalized radial electric field obtained from the numerical solution to Poisson's equation. The conditions are the same as there in Fig.3.

For gap widths satisfying the conditions, *s<<3.5 R_w*, *l_w>>R_w*, and *h_w=0*, it is found to within 3% accuracy electric field on the axis is given by [8]

$$E_z(0,z) = \frac{V(t)}{b}\exp\left[-\frac{\pi}{b^2}z^2\right], \qquad (8).$$

where, $b = 2R_w\left[0.73 + 0.53\left(s/2R_w\right)^2\right]$. Similarly, in the limiting case of very long washers with $l_w \to \infty$, and long vertical dimensions $h_w \to \infty$, the solution can be approximated to within 0.02% accuracy by [9]

$$E_z(0,z,t) = \frac{V(t)}{0.52R_w}\frac{1}{\left[2\cosh\left(1.57z/R_w\right)\right]^{1.54}}. \qquad (9)$$

All three solutions are compared with the numerical solution of Poisson's equation for the realistic parameters of the induction bunching module and are shown in Fig.3. As evident from Fig.3, all solutions give nearly identical results.

Profiles of the radial electric field for the conditions in Fig. 3 are shown in Fig.4. From Fig.4 it is evident that the radial electric field can be approximated as a linear function of radius, r for $r<R_w/3$. Because the beam radius in typical experiments is less than $R_w/3$, a linear approximation for the radial electric field as a function of r can be used to estimate the velocity change in the gap of the induction bunching module.

The linear part of the radial electric field near the axis can be calculated making use of the vacuum Poisson equation

$$\frac{1}{r}\frac{\partial(rE_r)}{\partial r} = -\frac{\partial E_z}{\partial z}, \qquad (10)$$

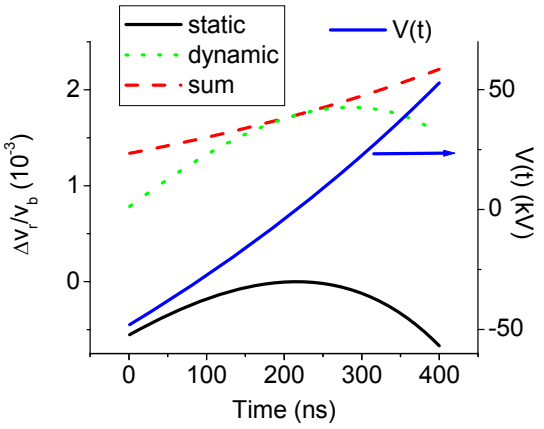

Figure 5: The static [black, solid curve, Eq.(15)] and dynamic aberrations [green, dotted curve, Eq.(13)] for the induction bunching module in the NDCX-I experiment. Blue curve shows the voltage pulse. Here, t_p=400ns, E_b=300keV, r=1cm, and R_w=3.8cm.

which gives, for $r << R_w/3$,

$$E_r = -\frac{r}{2}\frac{\partial E_z}{\partial z}, \qquad (11)$$

where the on-axis longitudinal electric field is given by Eqs.(7)-(9). The radial velocity acquired in the gap is then given by an integral over the ion beam trajectory in the gap, i.e.,

$$\Delta v_{br} \cong -\frac{e}{2}\int_{-\infty}^{\infty}\frac{dz\ r(z)}{M_b v_b(z)}\frac{\partial E}{\partial z}\left(z,0,t-\frac{z}{v_b}\right). \qquad (12)$$

The aberrations given in Eq.(12) can be split in two parts. One part corresponds to the "dynamic aberrations" associated with time change in the electric field during beam transport in the gap, and the second "quasi-static" part is independent of the voltage variation. For the dynamic part, in the limit where the ion time-of-flight through the gap, R_w / v_b, is short compared with the pulse duration in the induction bunching module, t_p, the time delay dependence, $t - z / v_b$, can be expanded in a Taylor series. Also in the linear approximation, when the velocity tilt is small, $\Delta v_b \ll v_{b0}$, the changes in beam radius and velocity can be neglected. Substituting any of the profiles in Eqs. (7)-(9) for the electric field, and the first term in the Taylor series, and integrating by parts then gives [4]

$$\frac{\Delta v_{br}}{v_{b0}} \cong -\frac{r}{4v_{b0}}\frac{e\dot{V}(t)}{E_b}, \qquad (13)$$

where super-dot indicates time derivative of the voltage, and $E_b = M_b v_{b0}^2 / 2$ is the initial ion beam kinetic energy. Static aberrations are second-order effects in the parameter $\Delta v_b / v_{b0}$, and both changes in the beam radius and the velocity need to be calculated [8]. The value of the static aberration is given by [8]

$$\frac{\Delta v_{br}}{v_b} \cong -\frac{3re^2}{16E_b^2}\int_{-\infty}^{\infty} dz\ E_z(0,z,t)^2 . \qquad (14)$$

For the profile given in Eq.(8) for the electric field, the static aberrations are found to be

$$\frac{\Delta v_{br}(r)}{v_b} \cong -0.082\left(\frac{eV(t)}{E_b}\right)^2\frac{r}{R_w}. \qquad (15)$$

Plots of both the static and dynamic aberrations are shown in Fig.5.

From Fig.5 it is evident that the aberration effects in the gap are much larger than the thermal (or emittance) effects, which are of order $v_{bT} / v_b \sim 10^{-3}$. Without any compensation for the aberrations, the dominant dynamic aberrations in the gap will result in a spot-size radius of order $r_{sp}^d \sim \Delta v_{br} t_f \sim (r_b / 4)(eV / E_b)(t_f / t_p)$. Substituting $t_p / t_f = v_b / \Delta v_b$ and $eV / E_b = 2\Delta v_b / v_b$, we obtain

$$r_{sp}^d \sim r_b / 2 . \qquad (16)$$

The estimate in Eq.(16) is consistent with the experimental observation that the beam can not be significantly compressed radially during simultaneous compression [7] without compensation for the aberrations.

There are several ways to mitigate effects of aberrations in the gap. These include: (a) install a specially-designed Einsel lens, that will correct the aberration effects [9]; (b) significantly reduce the radius of the beam before passing it through the bunching module; (c) use a strong focusing element at the end of the compression, that will focus beam ions coming from different radii to the same spot location, because the acquired radial velocity in the final focus element, rv_b / F, is much stronger than the radial velocity due to the aberration effects. The latter approach has been chosen for correction of the gap aberration, and will be further analyzed in the next section.

Focusing with a final focusing element

A final strong focusing element can significantly mitigate aberrations in the induction bunching module. Indeed, due to aberrations in the gap, the ions will arrive at different radial locations at the plane of the final focusing elements (a 8T solenoid in case of NDCX-I). However, independent of radius, the beam ions will be focused onto the same final focal plane. The small difference associated with the aberrations will yield a spot radius due to the aberration of $r_{sp}^d \sim \Delta v_{br} t_{F_2}$, where $t_{F_2} = F_2 / v_b$ is the time-of-flight

through the focal length of the final solenoid F_2. For NDCX-I parameters, the final focal length is about 10 cm, whereas the drift section L_f is 1-2 meters, yielding a factor of ten (L_f / F_2) reduction in the final spot radius due to aberrations in the gap, by making use of the final focusing element.

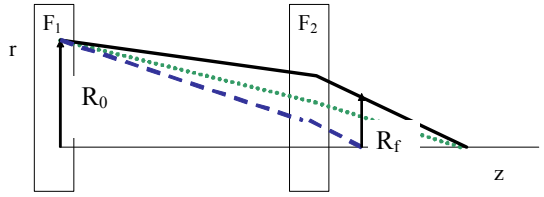

Figure 6: Schematic of the final focusing system consisting of a weak (F_1) and strong (final, F_2) solenoids. The green, dotted line shows the effect of aberrations in the induction bunching module; the blue, dashed line shows the chromatic effect due to the focal plane dependence on beam velocity.

However, the final focus includes chromatic effects due to the dependence of the final focal length on the beam velocity, $F \sim 1/v_b^2$. Taking into account chromatic effects, the spot size is determined by the change in the focal length $\delta F = 2F\Delta v_b / v_b$. From the geometrical relationship shown in Fig. 6, it is evident that the spot radius due to chromatic effects is given by $r_{sp}^f \sim r_f \delta F / F$, where r_f is the beam radius at the final solenoid, or equivalently,

$$r_{sp}^f \sim r_f \frac{2\Delta v_b}{v_b} \qquad (17)$$

From Eq. (17), it is evident, that the beam pulse has to arrive at the final focusing element with a small radius r_f in order to achieve a smaller beam spot radius r_{sp}^f. However, this radius cannot be too small, because the effective focusing in the solenoid has to be much stronger than the effects associated with the aberrations in the gap and the beam ion thermal effects or effective transverse emittance ($\varepsilon \approx v_T r_b$) [10], i.e.,

$$\frac{r_f}{F} \gg v_{br}^{abb}, \frac{v_T}{v_b} \approx \frac{\varepsilon}{v_b r_b} \qquad (18)$$

This condition limits the minimum value of r_f to $r_f \sim F/100 \sim 1mm$. It is possible to calculate exactly the optimum radius of the beam arriving at the final solenoid by determining the beam ion trajectories in the combined system consisting of two focusing elements.

If the beam exits the transport section with a converging angle r / F_1, the different parts of beam pulse will focus radially at different locations due to chromatic effects caused by the applied velocity tilt during the simultaneous longitudinal and transverse compression. This corresponds to effective errors in the beam radial velocity with $\delta v_r \sim v_b (r / F_1)(\delta F_1 / F_1)$, or $\delta v_r / v_b \sim (r / F_1)(\Delta v_b / v_b)$. These errors are larger or comparable with the aberration in the core. Therefore, in the subsequent analysis, we neglect aberrations in the induction bunching module and account only for chromatic effects in the two focusing elements. The general calculation, taking two focusing solenoids into account, gives for the beam spot radius at the target,

$$r_{sp} \sim \frac{r_b \Delta v_b}{v_b} \frac{F_2 F_1 + 2(F_1 - L)^2}{(F_2 + F_1 - L)F_1}, \qquad (19)$$

where L is the distance between the two focusing elements. Minimizing the final spot size with respect to L, we obtain

$$r_{sp,\min} = \frac{r_b \Delta v_b}{v_b} \sqrt{\frac{8F_2}{F_1}}. \qquad (20)$$

For NDCX-I parameters, $F_1 \sim 200cm$, $F_2 \sim 10cm$, and $\Delta v_b / v_b \sim 1/6$, Eq. (20) gives a value of the final spot radius corresponding to 1mm, which is 3-5 times smaller than the value without a final focusing element [compare Eq. (20) with Eq.(16)]. However, this estimate assumes complete neutralization of the ion beam space-charge. In the next section, we discuss the neutralization physics for an intense ion beam pulse.

NEUTRALIZATION PHYSICS OF INTENSE ION BEAM PULSE

The intense ion beam can be neutralized by emitting surfaces, hot filaments, or honeycomb grids inserted into the beam pulse. If the ion beam is neutralized by a localized source of electrons, the electrons are attracted by the ion beam space charge, and acquire an energy of order the ion beam self-potential. This self-potential is quite large for typical NDCX-I beam, from of order of $\Phi_b \sim 100$ V for an uncompressed beam, to of order 10 kV for a compressed beam pulse. As discussed above, the level of other aberrations is of order 3-10 times the thermal effects, for an ion beam temperature $T_b \sim 0.2$eV. Therefore, the degree of beam space-charge neutralization has to be extremely good, of order $1 - T_b / e\Phi_b$, or much better than 99.8%. To produce such a high level of neutralization, cold electrons have to be available everywhere on the beam path and provide efficient charge neutralization without being heated by the beam. *This requires that the drift compression region is fully filled by a background plasma everywhere along the beam path.* The beam current tends to be neutralized by the plasma electrons if beam radius is large compared with skin depth c / ω_{pe}, or a large external magnetic field is applied

[11,12]. The current neutralization condition corresponds to

$$\sum_{j=b,e,i} e_j v_j n_j = 0 , \qquad (21)$$

where v_j and n_j are the axial velocity and density of the various components (j=b,e,i) the beam density. The longitudinal electric field is given by momentum equation for the electrons

$$-eE_z = m_e v_b \partial v_b / \partial z . \qquad (22)$$

Therefore, the electric field tends to accelerate electrons in the beam head, and decelerate electrons in the tail. Correspondingly, it decelerates the beam ions in the beam head, and accelerates beam ions in the tail. The acquired ion beam momentum due to the self-fields is of order $\delta v_{bz}^p \sim m_e v_b t_f / t_p (n_b / n_p)$, where we have used the estimate that $\partial v_b / \partial z \sim 1 / t_p$. Substituting the relationship $t_p / t_f = v_b / \Delta v_b$, we obtain

$$\frac{\delta v_{bz}^p}{v_b} \sim \frac{m_e}{M_b} \frac{v_b}{\Delta v_b} \frac{n_b}{n_p} . \qquad (23)$$

Because the ratio of the electron to ion mass is very small, the self fields do not affect the longitudinal compression during beam propagation in the background plasma. Similarly, from radial momentum balance, it follows that the force acting on beam ions is given by [11,12, 13]

$$F_{br} = m_e v_b^2 \frac{1}{n_p} \frac{\partial n_b}{\partial r} . \qquad (24)$$

Therefore, the radial velocity acquired by the beam ions is $\delta v_{br}^p \sim F_{br} t_f / M_b$ or

$$\frac{\delta v_{br}^p}{v_b} \sim \frac{m_e}{M_b} \frac{L}{r_b} \frac{n_b}{n_p} \qquad (25)$$

For typical NDCX-I parameters, Eq.(25) gives $\delta v_{br}^p / v_b \sim 10^{-3}$, which is comparable with thermal effects, $v_{bT} / v_b \sim 10^{-3}$. Assuming that the plasma density higher is than the ion beam density everywhere helps reduce the force acting on the beam ions to negligible levels. However, the absence of sufficiently dense plasma even in one location can greatly reduce the neutralization, especially, in the presence of a strong applied magnetic field, in which the plasma can also support large radial electric fields [6,12].

CONCLUSIONS

The present analysis shows that there are several limiting factors that limit for simultaneous longitudinal and transverse neutralized compression. These are: (a) errors in the applied velocity tilt compared to the ideal velocity tilt, which correspond to all ions in the beam pulse arriving at the same location after compression. The longitudinal compression ratio is inversely proportional to the relative error [see Eq.(6)]; (b) radial compression is limited by chromatic effects in the focusing system and are proportional to the applied velocity tilt, as given in Eq.(20); and (c) background plasma can provide the necessary neutralization for compression, provided the plasma density exceeds the beam density everywhere along the beam pass, i.e., $n_p > n_b$. Insufficient plasma density at some location can result in a large self-electric field, preventing effective radial compression.

REFERENCES

[1] P.K. Roy *et al.*, Nucl. Instr. and Meth. in Phys. Res. A **577**, 223 (2007); P.K. Roy *et al*., Phys. Rev. ST Accel. Beams **9**, 070402 (2006).

[2] A. B. Sefkow *et al.*, Phys. Plasmas **16**, 056701 (2009).

[3] P. Seidel *et al.*, these proceedings (2009); P.K. Roy *et al.*, Phys. Rev. Lett. **95**, 234801 (2005).

[4] D. R. Welch, *et al*, Nucl. Instr. and Meth. in Phys. Res. A **577**, 231 (2007).

[5] H. Qin and R. C. Davidson, Phys. Rev. ST Accel. Beams **5** 03441 (2002).

[6] E. A. Startsev and R. C. Davidson, New Journal of Physics **6,** 141 (2004).

[7] R. C. Davidson and H. Qin, Phys. Rev. ST Accel. Beams **8**, 064201 (2005).

[8] A.B. El-Kareh "Electron beam, lenses, and optics", New York, Academic Press (1970).

[9] E.P. Lee, private communication (2008).

[10] J. J. Barnard *et al.*, Proceedings of the 2005 Particle Accelerator Conference, 2568 (2005).

[11] I. Kaganovich, *et al.*, Phys. Plasmas **8**, 4180 (2001); Phys. Plasmas **15**, 103108 (2008); Nucl. Instr. and Meth. Phys. Res. A **577**, 93 (2007).

[12] M. Dorf, *et al*., submitted for publication (2009).

[13] K. Hahn, E. Lee, Fusion Engineering and Design **32-33**, 417 (1996).